

Detailed characterization of neutron-proton equilibration in dynamically deformed nuclear systems

A. Rodriguez Manso, A.B. McIntosh, A. Jedele, K. Hagel, L. Heilborn, Z. Kohley, L.W. May,
A. Zarrella, and S.J. Yennello

We extend the study of neutron-proton (NZ) equilibration in dynamically deformed nuclear systems presented in [1] by investigating further the correlations between the two largest fragments produced in semi-peripheral collisions of $^{70}\text{Zn}+^{70}\text{Zn}$, $^{64}\text{Zn}+^{64}\text{Zn}$, $^{64}\text{Ni}+^{64}\text{Ni}$ and $^{64}\text{Zn}+^{64}\text{Ni}$ at 35 MeV per nucleon measured at the Cyclotron Institute at Texas A&M University. The extent of NZ equilibration is investigated using the rotation angle as a clock for the equilibration. Fragments which are initially dissimilar in NZ composition converge exponentially with consistent rate constants across a wide variety of reaction partners and systems, indicating the equilibration follows first order kinetics. The statistical and dynamical components are separated on average. The equilibration curve for the purely dynamical is consistent with the overall equilibration curve, indicating the robustness of the method to statistical contamination. A small systematic effect in the composition is observed for reactions of a relatively neutron poor projectile with a neutron-rich target, consistent with physical expectations. Equilibrium composition and rate constant values are extracted from the data. No significant differences in the rate constants are noted between systems of different initial composition. This work was recently published[2].

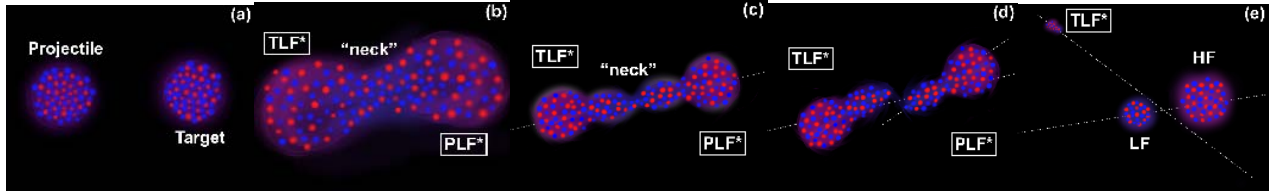


FIG. 1. Illustration of dynamical deformation and decay following a heavy-ion collision. Panel (a) shows a projectile approaching target. In panel (b), the projectile has rotated around the target forming a low-density “neck” region. In panel (c), the excited PLF* and TLF* have moved further away from each other and stretched into a “string of pearls” with the smallest fragments forming out of the neck region. Panel (d) represents the breaking of the nuclear system with the PLF* separating from the TLF*. Panel (e) shows the subsequent separation of the PLF* into HF and LF [3].

The general features of heavy-ion reactions near the Fermi energy proceeding through extremely deformed intermediate states are illustrated in Fig. 1[3]. Initially, there are the target and projectile, in panel(a), and a deeply penetrating contact between them with slight compression. As the excited Projectile-Like Fragment (PLF*) and excited Target-Like Fragment (TLF*) begin to separate from each other, in panel(b), a low-density neck of nuclear material is formed between them due to, in a classical description, nuclear viscosity and surface tension. Neutrons are driven preferentially to the low-density neck due to the density dependence of the asymmetry energy. This is illustrated in the figure by the excess of neutrons (in blue) in the neck and the relatively higher concentration of protons (in red) in the PLF* and TLF* regions. The velocity gradient stretches the system and the competition of the velocity

gradient with surface tension amplifies instabilities, panel(c); until the velocity gradient stretches the system beyond the capabilities of the nuclear force to hold it together and the system ruptures, panel(d). After one rupture of the neck, the now separated PLF* and TLF* are likely to be strongly deformed along the separation axis and, because of their deformation, they are likely to break again. The subsequent breakup of the PLF* into two pieces (the heavy fragment, HF, and the light fragment, LF) is illustrated in panel(e). If some time elapses between the PLF*-TLF* scission and the HF-LF scission, the angular momentum of the PLF* causes rotation through an angle so that the relative velocity of HF and LF makes a non-zero angle with the PLF*-TLF* separation axis, the center-of-mass velocity of the PLF*. If the angular velocity can be deduced and the breakup timescale is short relative to the rotational period, the rotation angle can be used as a clock. Since the neck is neutron rich at the time of the first scission, nucleon flow between regions of the deformed PLF* allow NZ equilibration to occur between the developing HF and LF. Thus measuring the composition of HF and LF as a function of the rotation angle allows direct observation of the time dependence of NZ equilibration.

Some highlights of the work involve the study of the PLF*'s deformation alignment. Representative angular distributions, α , are illustrated in the left panel of Fig. 2, for the $^{70}\text{Zn}+^{70}\text{Zn}$ system.

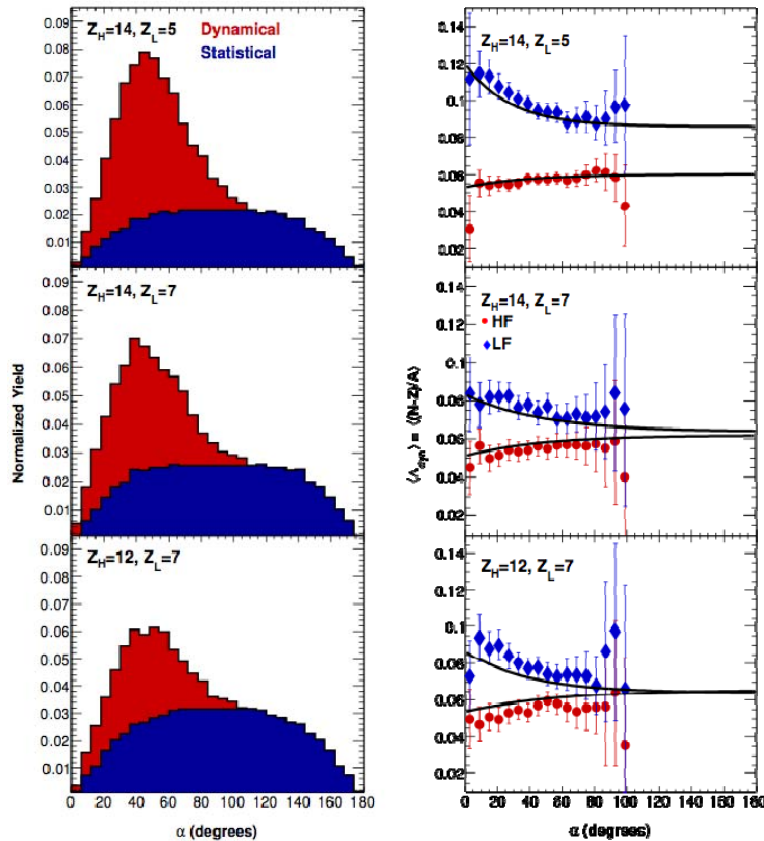


FIG. 2. System $^{70}\text{Zn}+^{70}\text{Zn}$, where three representative combinations of HF and LF are shown: $Z_H=14$, $Z_L=5$ (upper panel), $Z_H=14$, $Z_L=7$ (middle panel) and $Z_H=12$, $Z_L=7$ (lower panel). Left panel: normalized angular distribution α where the blue area represents the statistical contribution and the remaining area (red) represents the dynamical contribution. Right panel: Average dynamical composition, $\langle \Delta_{dyn} \rangle$, as a function of the decay alignment α . The black lines correspond to the exponential fit of the average composition as a function of the decay alignment.

Three representative combinations of HF and LF are shown. They are strongly peaked with $\alpha < 90^\circ$. The distributions fall toward 0 at $\alpha = 0^\circ$ and $\alpha < 180^\circ$, a consequence of the geometry of the detector array which gives a reduced detector efficiency due to double hits. This impacts particles at a particular angle α the same regardless of the mechanism of their origin. The total yield can be understood as arising from two different mechanisms of production: statistical decay and dynamical decay. The observed yield for $\alpha > 90^\circ$ comes primarily from statistical decays from a rotating source which produces an angular distribution that is symmetric about 90° . The excess observed yield for $\alpha < 90^\circ$ is consistent with dynamical decay, most probable at the smallest angles and steadily decreasing in probability with increasing angle.

In order to disentangle dynamical from statistical decay contributions to the yield, we describe the total yield as the sum of the statistical and dynamical components $Y_{total} = Y_{dyn} + Y_{stat}$. We assume the statistical yield is symmetric at about 90° and that the yield at large α (above 108°) is entirely statistical. Modeling the precise shape of the statistical component requires a detailed knowledge of the angular distribution of intermediate-mass fragments statistically emitted from a large nucleus for a range of angular momenta. We use instead our estimate of the statistical yield based on the measured yield at large α to show that our subsequent equilibration results are quite insensitive to the accounting of statistical decay. Our estimates of the statistical (in blue) angular distribution are shown in the left panel of Figure(2). The red area corresponds to the dynamical contribution.

Furthermore, we present a method to extract the dynamical composition as a function of α , describing the observed composition as a combination of the composition of the dynamical component and the statistical component, each weighted by their fractional yield as $\langle A \rangle = \langle A_{stat} \rangle f_{stat} + \langle A_{dyn} \rangle f_{dyn}$. We observe that the composition of the statistical component is independent of the angle for $\alpha > 100^\circ$, and assume that this is true also for $\alpha < 100^\circ$. This enables us to calculate $\langle A_{dyn} \rangle$ as a function of α , presented in the right panel of Fig. 2. Exponential fits from the overall composition are represented as black lines for easier visual comparison.

The LF (HF), which originates close to (far from) the neck region and therefore is neutron-rich (neutron-poor), starts off with a large (small) initial composition $\langle A \rangle$ for small alignment angles. As the angle of rotation increases, surface tension drives the system towards sphericity, keeping the HF and LF in contact longer, resulting in more time to exchange nucleons. The opportunity to exchange nucleons allows the asymmetry energy to drive a net neutron flow out of the LF and into the HF to equilibrate the chemical potentials of the two nascent fragments. This gives rise to similar values of the composition for the LF and the HF at higher alignment values. The $\langle A_L \rangle$ changes by a larger amount than the $\langle A_H \rangle$. This is a consequence of mass conservation, considering that the HF is larger than the LF and thus, the exchange of nucleons affects the composition of the latter more. The dynamical yield generally follows the same trend as the overall yield. The compositions are slightly more extreme for the purely dynamical component (i.e. the LF is slightly more neutron-rich and the HF is slightly more neutron-poor). It is not surprising that a statistical "background" of constant composition would mute the signal present in the purely dynamical. Applying this correction to isolate the dynamical component results in significantly larger uncertainties. The rate of change of the composition is essentially unaffected by the correction and the precise values of the composition are modified slightly. We continue the analysis on the inclusive composition rather than the dynamical, with the knowledge that the rates extracted are minimally

impacted by the statistical contribution, and our resulting uncertainties are minimized by avoiding the systematic uncertainty introduced by the subtraction.

We expanded our study to other projectiles and targets. The fits of $\langle A \rangle$ as a function of α are performed for thirty-two pairings of Z_H, Z_L for the $^{70}\text{Zn}+^{70}\text{Zn}$, and $^{64}\text{Zn}+^{64}\text{Zn}$ systems, for twenty-five pairings for the $^{64}\text{Ni}+^{64}\text{Ni}$ and for sixteen pairings for the $^{64}\text{Zn}+^{64}\text{Ni}$ asymmetric system. Fig. 3 shows the average composition $\langle A \rangle$ as a function of the decay alignment α for the $Z_H=12, Z_L=7$ pair in all the systems studied. From the comparison of the different panels it is observed that HF and LF for the $^{70}\text{Zn}+^{70}\text{Zn}$ and $^{64}\text{Ni}+^{64}\text{Ni}$ systems have $\langle A \rangle / \alpha$ correlations that are essentially the same. The $^{64}\text{Zn}+^{64}\text{Zn}$ is less neutron-rich than the other two symmetric systems. We see that the $\langle A \rangle / \alpha$ correlation is shifted to lower values (i.e. lower equilibrium composition) but the rate constant and the change from initial to final values are essentially the same. The comparison between the $^{64}\text{Zn}+^{64}\text{Zn}$ and the $^{64}\text{Zn}+^{64}\text{Ni}$ systems is quite interesting. The initial composition for the HF is essentially the same for the two, but the composition of the LF is significantly more neutron rich for the system with the more neutron-rich target. For both systems, the composition of HF and LF approach a common value, but this value is more neutron rich for the system with the neutron-rich target. While the magnitude of these shifts is not far from the statistical errors on each individual point, the systematic shift of all the points from one system

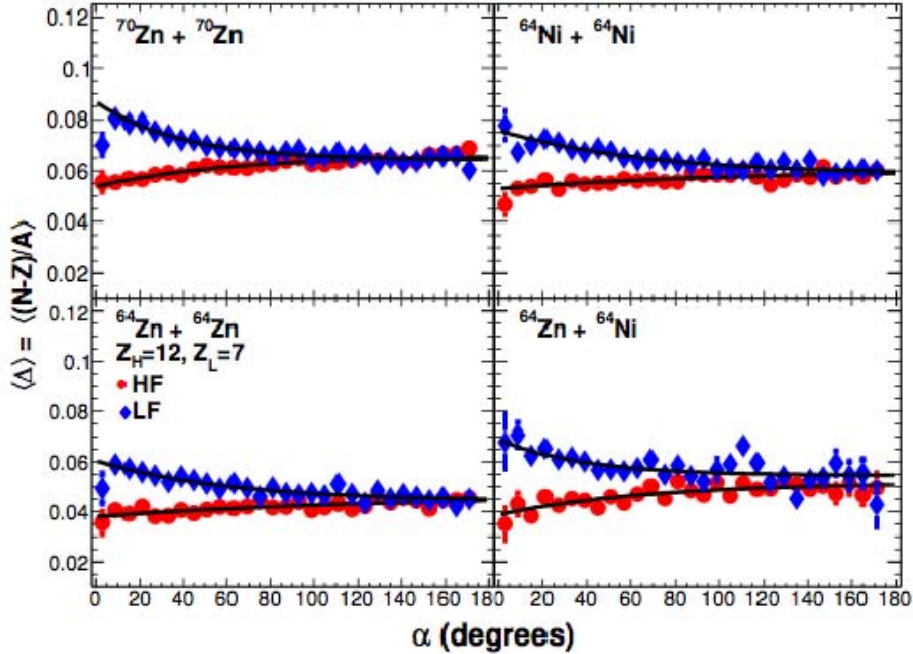


FIG. 3. Average composition $\langle A \rangle$ as a function of the decay alignment α for the $Z_H=12, Z_L=7$ pair in all systems studied (i.e. $^{70}\text{Zn}+^{70}\text{Zn}$, $^{64}\text{Zn}+^{64}\text{Zn}$, $^{64}\text{Ni}+^{64}\text{Ni}$ and $^{64}\text{Zn}+^{64}\text{Ni}$). The HF is represented in red circles and the LF in blue rhombi. The black lines correspond to the exponential fits of the data.

to the other is consistent with the expected effects of changing the neutron richness of the target. More details on these results have been published in [3].

- [1] A. Jedgele *et al.*, Phys. Rev. Lett **118**, 062501 (2017).
- [2] A. Rodriguez Manso *et al.*, Phys. Rev. C **95**, 044604 (2017).
- [3] A. Poulsen, oxidantshappencomics.wordpress.com, 2016.